Journal of Mining and Environment (JME) Vol. 13, No. 1, 2022, 33-51

Shahrood University of Technology
Iranian Society of Mining Engineering (IRSME)

Journal of Mining and Environment (JME)

journal homepage: www.jme.shahroodut.ac.ir

# Mineralogical Approach-A Tool for Geo-Metallurgical Prediction of Tizert Copper Deposit (Ighrem Inlier, Anti-Atlas, Morocco)

Kaoutar Dachri[1*], Khalid Naji[2], Keltoum Nouar[2], Intissar Benzakour[2], Khalid Ouzaouit[2], Mustapha Badri[2], Abdelmalek Boussetta[2], Hakim Faqir[2], Khalid El Amari[1], and Mohammed Hibti[1]

*1- Caddi Ayyad University, FST Marrakech, Moroccan*
*2- Reminex reaserch Center, Moroccan*

## Article Info

*Received 15 January 2022*
*Received in Revised form 12 March 2022*
*Accepted 15 March 2022*
*Published online 15 March 2022*

*DOI:10.22044/jme.2022.11576.2144*

## Keywords

*Automated quantitative mineralogy*
*Tizert*
*Copper*
*Geometallurgy*
*Morocco*

## Abstract

This work aims to define an efficient and innovative tool in order to make early metallurgical predictions of the Tizert deposit in western Anti-Atlas-Morocco. To do this, the mineralogical approach is used as a tool of geometallurgical prediction using a combination of the lithological field observations on representative drill cores, microscopic characterization performed on 54 thin sections, and automated quantitative mineralogy (AQM) conducted on five composite samples. The metallurgical prediction of the Tizert ore is based on the liberation data, notably on the copper content locked in the gangue and on unrecoverable copper buried as a solid matrix in the gangue minerals (refractory copper). In order to ensure the validity of the proposed method, the results of mineralogical prediction are compared with the flotation test work performance. As a result, the predicted copper recovery results from the mineralogical data are practically the same as those obtained through the flotation tests, showing a maximum difference of 2.02%, an R2 value of 0.96, and a Root Mean Square Error of 1.64%. These results indicate that using the AQM data, the copper recovery could be predicted accurately for the Tizert ore. Furthermore, an early prediction of the flotation performance is very useful in the geo-metallurgical model conception. In addition, such an approach ensures visibility throughout the life of the mine, and provides quick and cost-effective data for processing the performance. On an industrial scale, the applicability of this method can be expanded further by integrating the mineralogical approach into all steady-state processes in order to cover the possible mineralogical variety during the operations, and ensure an industrial process control.

## 1. Introduction

In the mining industry, mineralogy has become an important tool in geo-metallurgical studies. Understanding bulk mineralogy is fundamental when making metallurgical predictions. Such an approach ensures visibility throughout the life of the mine, and provides a quick and cost-effective data for the processing performance.

Geometallurgy is a multi-disciplinary science that combines the geological and metallurgical information necessary for the production and management of the mining operations [1]. It aims to define the geological, mineralogical, and geochemical variables existing within a mineralized envelope that could affect metallurgical processing throughout the mining chain (process suitability, performances, recovery, products quality …). The industrial application of geo-metallurgy, called a geo-metallurgical program, is composed of three types of programs: traditional, proxy, and mineralogical [2].

The traditional approach is based on the chemical assays. The recovery is a function of the chemical composition of the ore. The proxy program uses the geo-metallurgical tests in order to characterize the

Corresponding author: dachri.kaoutar@gmail.com (K. Dachri).

metallurgical behavior of the ore in the processing stages. The mineralogical approach is when the geo-metallurgical program is largely based on the mineralogical data [2]. It corresponds to a continuous and systematic collection of quantitative mineralogical information [3].

The application of a mineralogical approach has increasingly been used to investigate the metallurgical performance, and predict the recovery of copper bearing minerals [4–6]. The flotation recovery of sulfide ore in a sediment-hosted copper-cobalt deposit in the Democratic Republic of Congo has been predicted by the correlation of mineralogical data delivered by the quantitative mineralogy analysis and the flotation test work [4]. The prediction of flotation recovery of copper sulfosalts has been ensured through an integrated mineralogical approach by the implementation of the principal component analysis for linking the flotation and mineralogical characteristics (modal mineralogy, grain size, and liberation degree) of the feed samples [5]. At the Kansanshi mine, in the Northwestern Province of Zambia, it has been demonstrated that the quantitative mineralogical data is critical in understanding the previous recoveries and predicting copper recovery [6].

This paper explores the use of the mineralogical approach for the geo-metallurgical prediction of the Tizert copper deposit, in the western Anti-Atlas-Morocco, in order to anticipate and predict the metallurgical performance of Tizert ore, reduce the exploration costs, and provide a tool for the eventual evaluation of the metallurgical performance. For this aim, this work was based on a combination of lithological field observation, microscopic characterization, and automated quantitative mineralogy analysis. In order to ensure the validity of the proposed method, the results of the mineralogical prediction were compared with the flotation test work performance.

## 2. Geological Setting

Tizert is a sedimentary copper deposit [7−10]. It is one of the largest sediment-hosted deposits in Morocco [9]. The site is located 160 km south-east of Agadir (Figure 1-A), with resources estimated to be 56,820,000 t with 1.03% Cu and 23 g/t Ag [10].

On a regional scale, the Tizert area is situated at the northern border of the Igherm inlier (Western Anti-Atlas), which consists of a Paleoproterozoic basement and a Neoproterozoic cover [11]. The Paleoproterozoic substratum is mostly composed of granites, migmatites, and mica schists [12], while the Neoproterozoic cover consists of three distinct lithologies: (i) Cryogenian quartzites and calcarous beds [13], (ii) Lower Ediacaran formations primarily composed of conglomerates and volcanoclastics with interbeds of pelites and sandstones [14], and (iii) Upper Ediacaran units composed of andesite flows surmounted by pelites and conglomerates [15].

The Tizert deposit is hosted by the Ediacaran sedimentary formations on a local scale. The lithological succession consists of three lithostratigraphic units [8]. From the base to the top (Figure 1-C):

- Lower Ediacaran Tiddiline unit (600 Ma [16, 17]), considered the basement. It is composed of conglomerates including decimetric to metric pebbles cemented together by a clay matrix.

- Basal Series was deposited between the Late Ediacaran and the Early Cambrian (between 550 ± 3 Ma and 521 ± 7 Ma [18]). It is composed of two silicoclastic units, the basal conglomerate at the base and the sandstones at the top, separated by the Basal Limestone unit.

- The lower limestone unit corresponds to the Ediacarian/Cambrian transition (534 ± 10 Ma [19]). It is characterized by silicified dolostone beds, surmounted by stratified limestone, referring to the Tamjout Dolomite formation [9, 20].

### 2.1. Mineralization

The economic mineralized zone extends laterally for more than 5 km with a thickness of 45 m along the Basal Series and the Tamjout Dolomite [9]. Three stages of mineralization were difined in the Tizert area [7, 9] :

- Primary mineralization, represented by sulfides occuring as dissemination in sandstone, microconglomerates, and siltstones. The mineral assamblage is composed of pyrite, chalcopyrite, bornite, and chalcocite.

- Secondary mineralization stage that figures as vein mineralization type, fills the fractures, and veins crossing the sedimentary layers of the Basal Series. This type of mineralization can be found in the Tamjout Dolomites and the Tiddline conglomerates underlying the Basal Series unit. The mineral pargenesis is composed of pyrite, chalcopyrite, bornite, and chalcocite. The sulfide minerals are associated with dolomite, calcite, sericite, and chlorite [9] .

- Mineralization from supergene alteration. The alteration phase affects the vein and stratiform mineralization, generating chalcocite, covellite, native copper, and malachite paragenesis [7]. Supergene alteration is abundant along the contact between the Basal Series and the Tamjout Dolomites.

Textural characteristics of the Tizert mineralization show an association of disseminated sulfide with sedimentary structures (lamination and cross-stratifications), allowing the affiliation of the mineralization to the stratiform system hosted by the terminal Neoproterozoic-Lower Cambrian sedimentary formations [7, 9, 10].

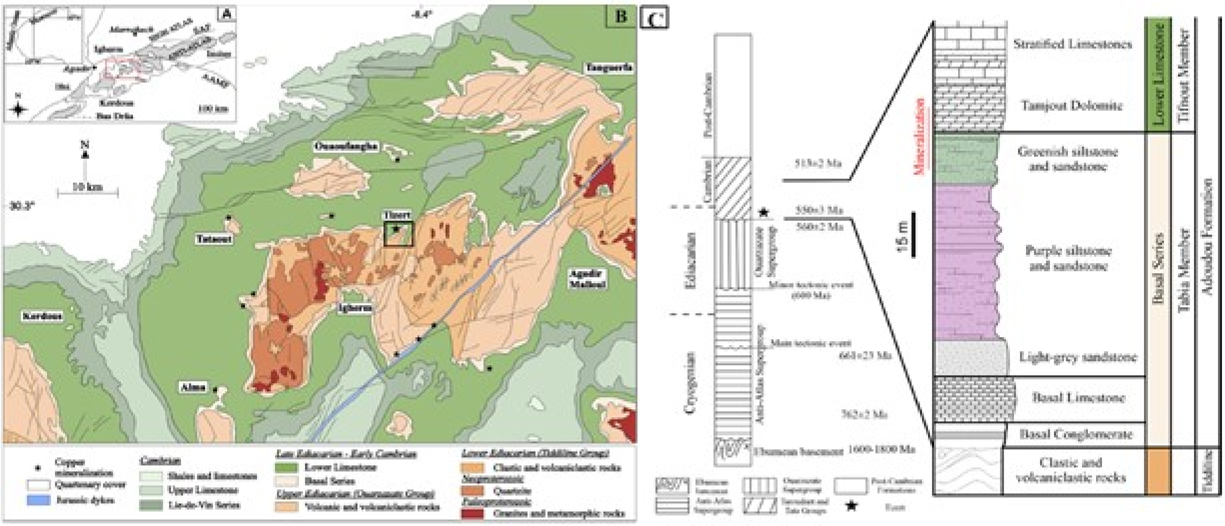


**Figure 1. A) Anti-Atlas general map; B) Geological location of Tizert deposit; C) Anti-Atlas synthetic lithostratigraphic columns (left) and major geological units observed in Tizert deposit (right) [9, 21].**

## 3. Materials and methods

### 3.1. Lithological observation

The current work is based on the lithological, mineralogical, and geochemical field data. The approach used to produce the geo-metallurgical data was first the characterization, in detail, of a number of representative samples from each geological zone of the deposit. The lithological observations were performed on seven representative drill cores and an N-S cross section in order to elucidate the spatial distribution of lithofacies, evolution of mineralization, and track the impact of the host rock on the mineralized facies of the Tizert deposit.

### 3.2. Optical and SEM microscopy

The optical and standard electron microscopy (SEM) were completed on 54 thin sections, selected from the representative drill cores to reflect the mineralization character of the Tizert deposit. The characterization was performed using an Olympus microscope and conventional SEM Philips XL 30 equipped with a Bruker Quantax X-Flash 6130 energy dispersive X-ray (EDX) detector for semi-quantitative analysis.

### 3.3. Compositing operation

The compositing operation was the next step following the thin section study. The purpose was to explore the behavior of the mineralization by taking into consideration the evolution of the casing, reducing the number of samples, making the processing easier, and limiting the processing routes.

The composites were made from the representative drill cores throughout the deposit. In order to determine the feasibility of drilling in the Tizert deposit, the ordinary kriging method based on the lithogeochemical parameters was employed [22]. In addition, the delimitation of target parameters was based on the facies of the casing (Basal Series or Tamjout Dolomite) and the mineralization type (Sulfides, oxides or carbonates). The composites were generated using yardage-weighted drill core samples with a cut-off grade set at 0.3% Cu.

Based on the evolution of mineralization and the casing through the mineralized zones of the Tizert deposit, five composites, namely C1 to C5, were produced (Figure 2).

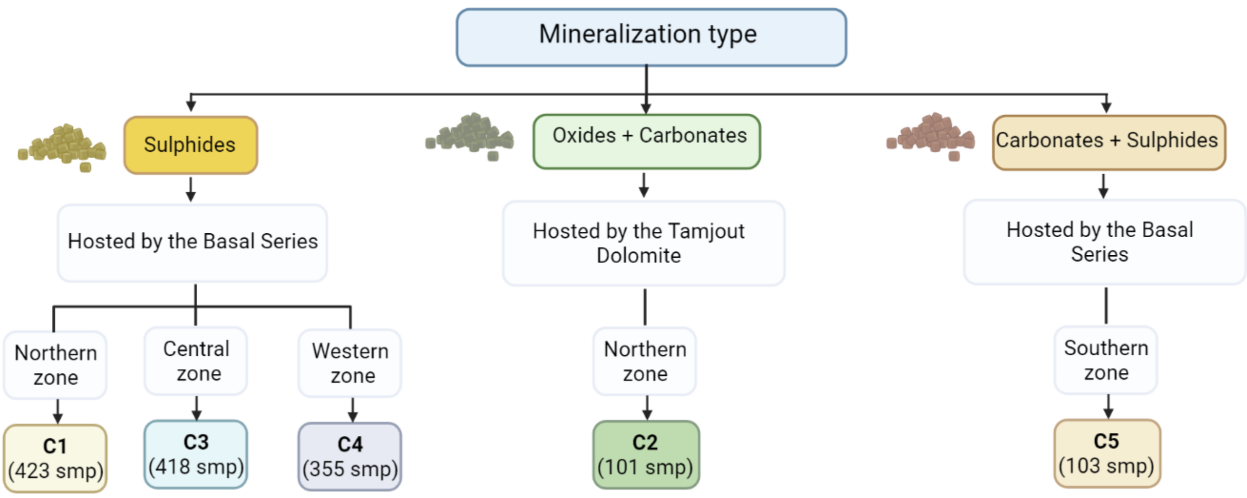


**Figure 2. Compositing operation according to mineralization type (smp: samples).**

### 3.4. Automated quantitative mineralogy analysis

The principal method of analysis employed in this work is automated quantitative mineralogy (AQM). This has been completed on polished thin sections from composite samples, in order to produce the quantitative mineralogy data (modal mineralogy, elemental deportment, and liberation). Each composite was ground to a $P_{80}$ of 120µm, then divided into four size fractions (+112 µm, -112/+75 µm, -75/+45 µm, and -45 µm). Graphite was used in the preparation of samples in order to disperse the particles, minimize settling, and segregation due to different mineral specific gravities. AQM was carried out at the REMINEX research center (Industrial complex of Guemassa, Morocco) using a Carl Zeiss Sigma VP automated scanning electron microscope instrument, equipped with Bruker detectors. The mineralogical data was processed using the Mineralogic software.

### 3.5. Geochemical analysis

Inductively coupled plasma optical emission spectroscopy (ICP-OES) was used to accomplish the geo-chemical investigation on the composite samples. For this aim, an Agilent 511 ICP-OES analyzer was used.

### 3.6. Flotation test

The flotation test work was conducted on the composite samples in order to establish the validity of the proposed method. The mineralogical characterization of the Tizert ore has revealed two kinds of copper deportment: sulfides and oxides. In order to ensure copper recovery from a mixed sulfide-oxide copper, the flotation test work was performed in two steps: ordinary flotation of sulfide and sulphidization of the oxidized fraction. According to lab-scale conditions, the composite samples were crushed into 120 µm through two stages of laboratory crushing, comprising jaw, and roll crushers as well as ball mill grinding.

The flotation experiments were carried out in a laboratory Metso flotation machine with an impeller speed adjusted to 1200 rpm. In each flotation test, 1 kg of the composite sample was placed in a flotation cell with a 2.4-L capacity. The system was floated at natural pH, ambient temperature, and a pulp density of 33% solids. The tests on the sulfide fraction were conducted using potassium amyl xanthate (PAX) as a collector, and methyl isobutyl carbinol (MIBC) as a frother. Sodium hydrogen sulfide (NaSH) was utilized as a sulphidizing reagent for the oxidized fraction, with potential control during the sulphidization process. For both the sulfide and oxide circuits, the flotation test comprised the rougher and scavenger phases (Figure 3). An overview of the optimal operating conditions for the flotation experiments is given in Table 1 (conditioning time, flotation time, and reagent concentrations). After each experiment, the sulfide and oxide concentrates were collected, dried, weighted, and analyzed for copper content. The results were combined into one cumulative concentrate.

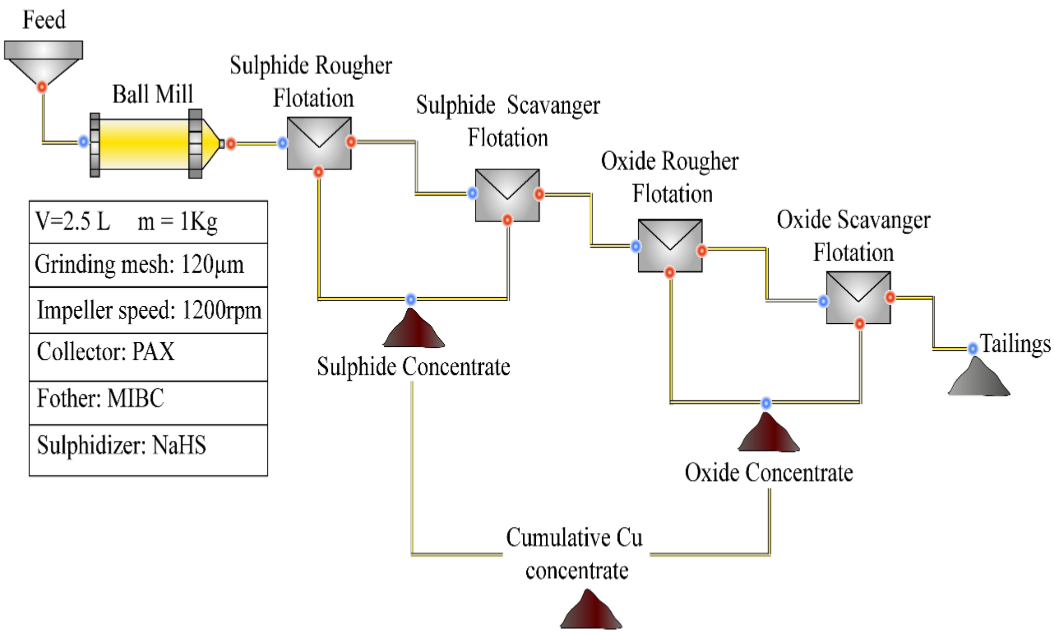


**Figure 3. Simplified flowsheet used throughout flotation experiments of Tizert ore.**

**Table 1. Flotation procedure for experiments described in this work.**

| Circuit | Stage | Conditioning time (min) | Flotation time (min) | Dosage (Range) |
|---|---|---|---|---|
| Sulfide | Frother adding | | | 40g/t |
| | Conditioning collector | 1 | | 40-50g/t |
| | Concentrate 1 | | 2-4 | - |
| | Concentrate 2 | | 2-4 | |
| | Concentrate 3 | | 2-4 | |
| Oxide | Sulphidization | 2 | | Controlled by the potential |
| | Conditioning collector | 1 | | 50-100g/t |
| | Concentrate 4 | | 2-4 | - |
| | Concentrate 5 | | 2-4 | |
| | Concentrate 6 | | 2-4 | |

## 4. Results and Interpretation

### 4.1. Lithological description

The lithological description of the studied drill cores shows three distinct lithofacies occurring at varying degrees of abundance (Figure 3). From the base to the top, one can notice:

- Conglomerate of the Tidiline formation (Lower Ediacaran), considered as the basement. It is composed of polygenic conglomerates that contain elements of old facies, pelites, granites, and quartzites, with a matrix composed of clay.

- The second lithofacies consists of repeating sandstones and conglomerate-sandstone beds, which laterally extend for tens to hundreds of meters. These recurrences represent the Basal Series unit (Late Ediacaran and Early Cambrian). The general composition of the conglomerates is represented by angular to surrounded fragments of granite, quartzite, andesite, and trachytes. The clasts are cemented by sandstones with a quartz-sericite-chlorite matrix. The basal conglomerate is interpreted as a fluvial system or delta developed along a lacustrine edge [23]. The sandstones are composed of metric lenticular sandstone beds showing cross-stratifications and paleocurrent undulations. The petrographic composition is represented by quartz, feldspars, and muscovite cemented by carbonate. The sandstone facies was interpreted to have been deposited in a fluvial system [24].

- Carbonate unit (Ediacarien/Cambrian transition): it is a massive carbonate sequence, cliff-forming, about tens of meters thick, overlying the Basal Series unit. The lithofacies are composed of limestone and dolomites referring to the Tamjout Dolomite formation (Early Cambrian).

The correlation of the studied drill core showed that the mineralized horizons were mainly localized in the Basal Series (Figure 4). The thickness of sediments and spatial distribution of sedimentary facies strongly depend on the topography of the basin controlled by depositional tectonic.

The mineralized facies of the Tizert deposit has four morphological aspects according to the host rock (Figure 5):

- Massive in the Basal Series conglomerates by filling quartz cavities in sandstone and carbonates or lodging the joints and interstices left between conglomerate clasts;
- Disseminated following the bedding of sandstones;
- Stratified in the carbonate formation;
- Fissural by sealing cracks in the Basal Series formations.

The main ore minerals identified were chalcopyrite, bornite, chalcocite, and malachite.

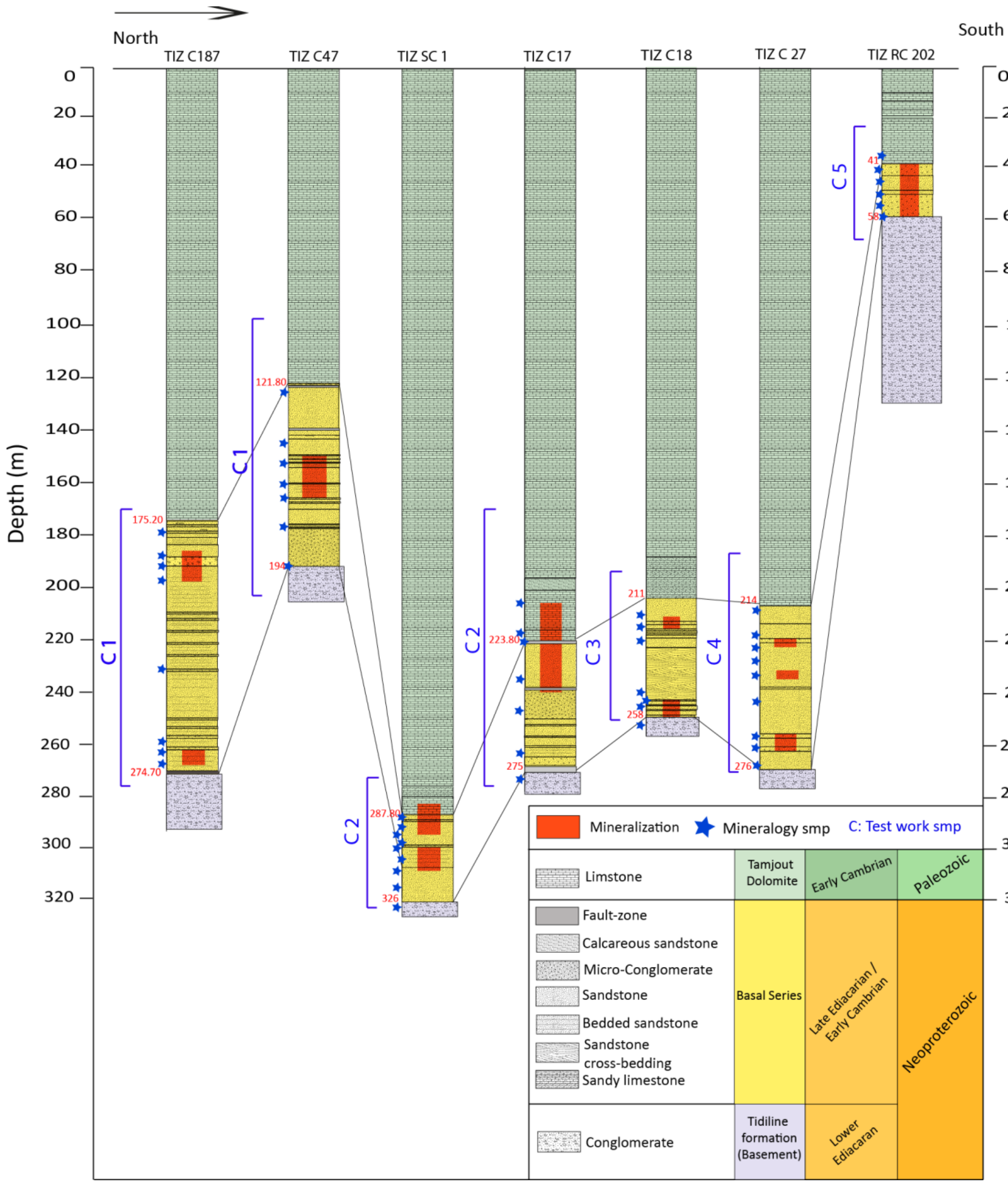


**Figure 4. North-south stratigraphic correlation for studied drill cores, with the placement of samples destined to petrographic study (mineralogy smp) and composite samples for the metallurgical test work (test work smp). Smp: samples; C: composite samples.**

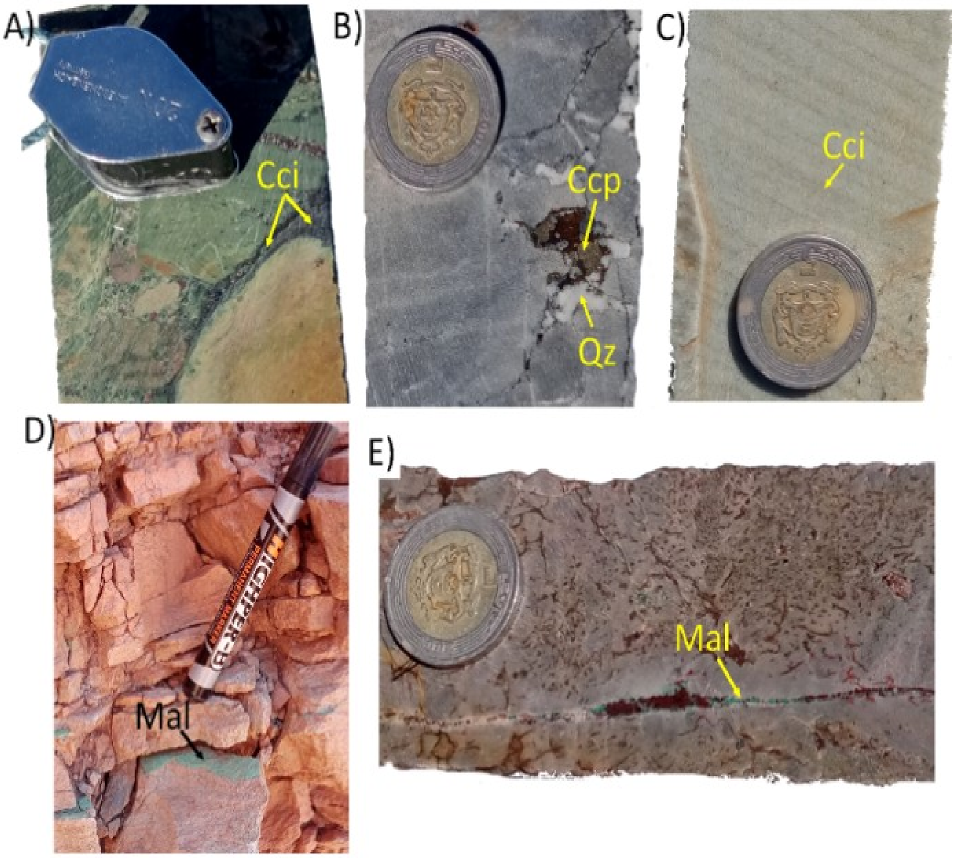


**Figure 5. Macroscopic observations of mineralized facies. (A) Massive chalcocite filling interstices between conglomerate elements. (B) Chalcopyrite fills quartz cavities in sandstone. (C) Fine chalcocite disseminations following sandstone bedding. (D) Malachite following stratification of limestone. (E) Fissural malachite seals oxidized facies cracks.**

## 4.2. Petrographic observations

The petrographic observations revealed a large variability of copper deportment represented by sulfides (chalcopyrite, bornite, chalcocite, and covellite) and copper carbonates (malachite). The paragenetic associations and replacement textures of copper deportment are illustrated in Figure 6.

**Chalcopyrite (CuFeS2)**, considered a primary sulfide, is one of three principal copper sulfides in the Tizert deposit. Chalcopyrite occurs as disseminated and massive grains in quartz vacuoles and dolomite. It could be affected by micro-fractures filled with chalcocite, covellite or iron oxide. Chalcopyrite commonly replaces pyrite grains, generating exsolutions of pyrite (Figure 6-A). According to the maps of elemental concentrations produced by SEM, silver was detected as a trace in the chalcocite crystal.

**Bornite ($Cu_5FeS_4$)** is identifiable under a microscope by its pinkish and violet colors in various shades. It is found replacing chalcopyrite or being altered to chalcocite and covellite. Bornite figures as disseminated or massive grains depending on the host-rock.

Chalcocite (Cu2S) is the most abundant copper-bearing mineral in the Tizert ore. It generally occurs as disseminated grains (5-10 µm) flowing through the bedding of sandstone, less frequently as massive aggregates in the conglomerates or filling cracks in the mineralized horizons of the Basal Series. In most cases, chalcocite is observed as a product of the replacement, partially or immediately, of chalcopyrite or bornite. Many types of replacement textures were identified including: rim, pseudo-morph, relicts, vein replacement, and myrmekitic texture. Near the surface, chalcocite is often associated with malachite.

**Covellite (CuS)** is an accessory mineral in the Tizert deposit. It occurs as disseminated grains, and replaces other sulfide minerals such as chalcopyrite (along grain edges), bornite, and chalcocite by adopting a lamellar texture (Figure 6-F).

**Malachite ($CuCO_3$, $Cu(OH)_2$)** is a secondary mineral found on the surface of mineralization areas. It is generated by the weathering and oxidation of copper-sulfide minerals, commonly called the supergene alteration process. Microscopic observations of the samples show that the malachite, in many cases, accompanies and surrounds chalcocite dissemination. Malachite occurs as massive grains in conglomerates and quartz cavities, disseminated or fissural in the sandstone and stratified in the carbonates.

Based on the microscopic and textural observations, three stages of mineralization were recognized. The first hypogene stage comprises Cu-Fe minerals, and is characterized by chalcopyrite and pyrite. The second hypogene stage includes secondary minerals such as bornite, chalcocite, and covellite. The final stage of mineralization is a supergene enrichment stage represented by malachite and iron oxide/hydroxide.

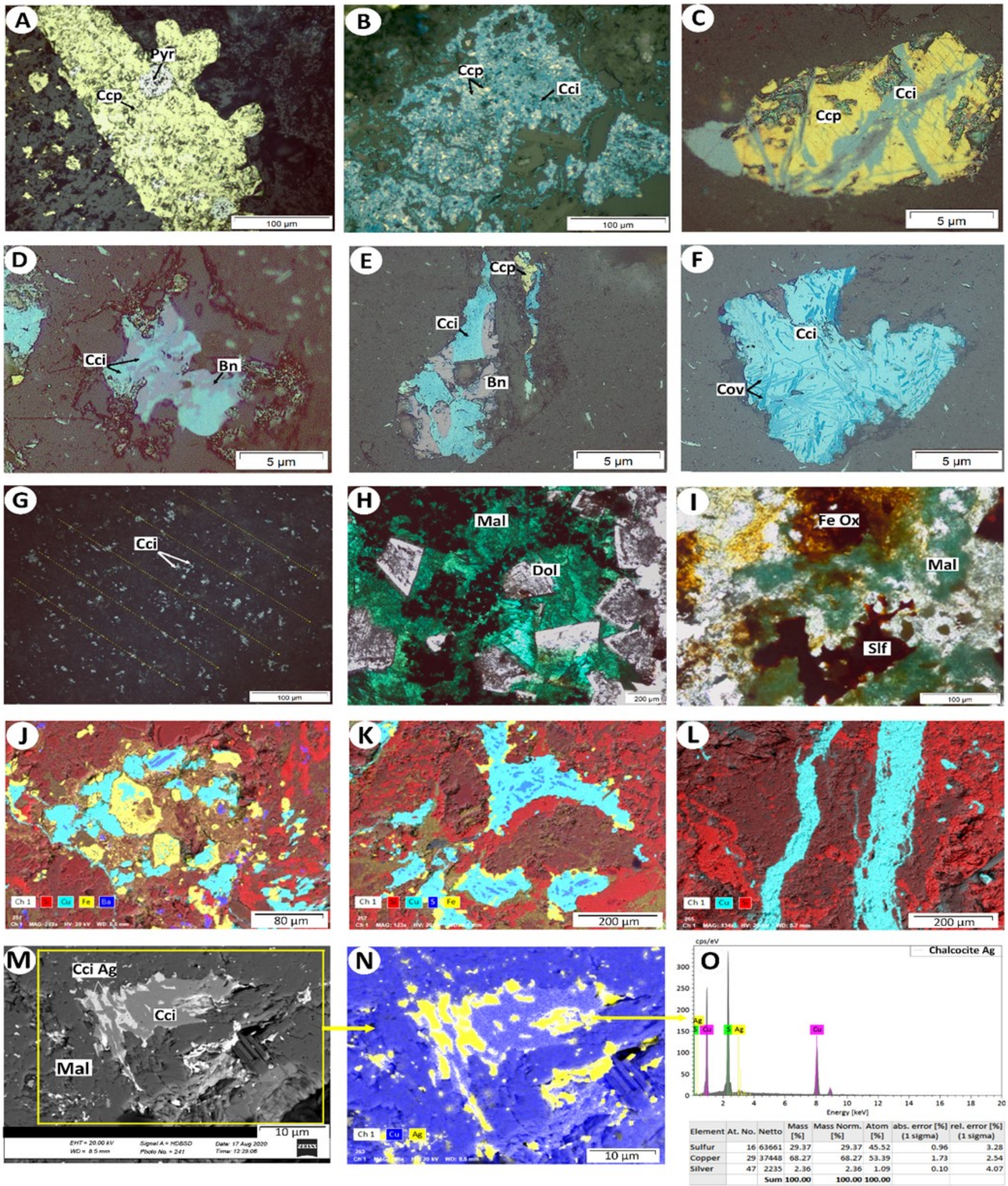


**Figure 6. Photomicrographs and elemental maps of various types of ore textures. A) Pyrite relicts replaced by chalcopyrite. B) Chalcocite with chalcopyrite relics. C) Chalcocite replaces chalcopyrite along irregular fractures. D) Chalcocite-bornite intergrowth. E) Bornite-chalcocite intergrowth; F) Lamellar covellite replacing chalcocite. G) Fine chalcocite dissemination flowing the bedding of sandstone; H) Massive malachite hosted in carbonate. J) EDS mapping of copper-bearing disseminated texture in silicate gangue. K) EDS mapping of a copper deportment hosted in silicates with a massive texture. L) EDS mapping of the copper deportment's fissural texture. (M) BSE photomicrograph of chalcocite containing a trace of silver. The whole is hosted in malachite. N) Elemental concentration map of chalcocite with a trace of silver. O) EDS quantification of chalcocite with a trace of silver. Ccp: chalcopyrite; Cci: chalcocite; Bn: bornite; Cov: covellite; Pyr: pyrite; Mal: malachite; Fe Ox: iron oxide/hydroxide; Slf: sulfide; Cci Ag: chalcocite with trace of silver.**

### 4.3. Geochemical analysis

The major and trace element abundances of composite samples are given in Table 2. The geochemical analysis refers to a silico-carbonate gangue for the analyzed samples. The $SiO_2$ content of samples C1, C3, C4, and C5 ranges from 13.65% to 52.33%. Their $Al_2O_3$, MgO, and CaO contents show a quite variable range: 7.76%–8.52%; 7.03%–8.44%; and 9.45%–10.45%, respectively. In the C2 sample, the low rates of $SiO_2$ (13.65%) and $Al_2O_3$ (1.61%) were compensated by the contents of CaO (24.56%) and MgO (17.23%), the principal elements constituting carbonate rocks (dolomites).

The range in copper content is from 1.09% to 1.12% for the analyzed samples. Considered as a bonus element, the silver content varies from 19.03 g/t to 28.01 g/t, and averages 23.17 g/t. A strong correlation is noted between silver and copper. This indicates the tendency for samples richer in copper to carry greater amounts of silver. This finding supports that of a mineralogical study conducted by SEM, and shows that silver is carried as a trace in sulfides (chalcocite) of the Tizert ore.

**Table. 2. Major and trace element analysis of composite samples.**

| Elements | *C1* | *C2* | *C3* | *C4* | *C5* |
|---|---|---|---|---|---|
| $SiO_2$ (%) | 52.33 | 13.65 | 50.68 | 54.4 | 39.95 |
| $Al_2O_3$ (%) | 8.03 | 1.61 | 7.58 | 8.52 | 7.76 |
| MgO (%) | 7.47 | 17.23 | 10.42 | 7.03 | 8.44 |
| $Fe_2O_3$ (%) | 1.67 | 2.73 | 1.96 | 1.17 | 2.57 |
| CaO (%) | 10.45 | 24.56 | 9.9 | 9.9 | 9.45 |
| $Na_2O$ (%) | 0.50 | 0.03 | 0.41 | 0.29 | 0.45 |
| $K_2O$ (%) | 2.25 | 0.43 | 2 | 2.63 | 2.08 |
| MnO (%) | 0.34 | 0.54 | 0.29 | 0.28 | 0.24 |
| $TiO_2$ (%) | 0.47 | 0.12 | 0.4 | 0.4 | 0.41 |
| $P_2O_5$ (%) | 1.15 | 0.24 | 0.44 | 0.57 | 0.34 |
| LOI (%) | 14.00 | 37.42 | 14.38 | 13.32 | 26.73 |
| Cu (%) | 1.11 | 1.12 | 1.10 | 1.09 | 1.09 |
| Ag (g/t) | 28.01 | 20.00 | 26.20 | 19.03 | 22.60 |
| As (g/t) | 42 | 486 | 300 | 80 | 100 |
| Au (g/t) | 0.05 | 2.09 | 0.05 | 0.07 | 0.05 |
| B (g/t) | 44 | 19 | 64 | 104 | 43 |
| Ba (g/t) | 1910 | 1115 | 1528 | 3364 | 1712 |
| Be (g/t) | 3 | 4 | 0 | 4 | 1 |
| Bi (g/t) | 10 | 10 | 10 | 10 | 10 |
| Cd (g/t) | 4 | 6 | 2 | 2 | 2 |
| Co (g/t) | 39 | 99 | 30 | 127 | 65 |
| Cr (g/t) | 146 | 154 | 150 | 206 | 176 |
| F- (g/t) | 430 | 317 | 630 | 495 | 617 |
| Ge (g/t) | 37 | 19 | 10 | 46 | 10 |
| Mo (g/t) | 8 | <8 | <8 | <8 | <8 |
| Ni (g/t) | 137 | 231 | 48 | 238 | 64 |
| Pb (g/t) | 146 | 288 | 183 | 31 | 73 |
| Sb (g/t) | 32 | 32 | 32 | 32 | 32 |
| Sn (g/t) | 22 | 51 | 185 | 29 | 294 |
| Zn (g/t) | 119 | 566 | 335 | 77 | 82 |

### 4.4. Automated Quantitative Mineralogy

For each composite sample, automated quantitative mineralogy (AQM) was performed on four size fractions (+112 m, +75 m, +45 m, and -45 m). The samples were produced as polished thin sections, and analyzed using the Mineralogic software. The creation of mineralogical recipe for the samples has for input the mineralogical data delivered by qualitative mineralogy (petrographic microscopy and SEM). The results were represented by a reconstructed sample representative of the size fractions of composite samples. The overall reconstructed value for samples was calculated by Mineralogic reporter taking into consideration the mass proportion of each size fraction relative to the overall sample.

#### 4.4.1. Mineral abundance

The modal mineralogy of composite samples is presented in Table 3. Overall, the main gangue minerals present in all samples are quartz (11.5%–

41.6%) and dolomite (19.5%–75%). Dolomite seemed to be more abundant in the sample C2 (75%). The mica content varies between 1.2% and 15% (1.4%–5.8% muscovite), the orthoclase amounts to 15%, while the chlorite and calcite present a maximum of 7.2% and 6.3%, respectively. All the other silicate and oxide minerals such as kaolinite, albite, goethite, and hematite constitute less than 4%. The copper deportment identified corresponds to sulfide, represented by chalcocite (0.2%–1.6%), bornite (0.1%–0.9%), chalcopyrite (0.2%–0.3%), with a small amount of covellite (0.1%–0.5%); carbonate defined by malachite (0.3%–1.6%); oxide expressed by cuprite (0.1%–0.3%), native copper (0%–0.1%), and iron oxide with a trace of copper (0.1%–1.5%).

Twenty-four minerals were detected in total, of which those present in trace quantities, notably pyrite, sphalerite, apatite, barite, rutile, and titanite, were grouped as "others" in Table 3.

The characterization of the copper deportment has revealed a progressive sequence of copper-enriched minerals, commencing with the replacement of chalcopyrite by bornite. Then bornite is progressively replaced and enriched in copper by chalcocite and covellite [25]. Near the surface, the oxide mineral (cuprite) probably formed fairly early in the sequence, together with iron oxide/hydroxide (hematite and goethite), while the carbonates (malachite) may have developed over a wide range of time.

**Table 3. Modal mineralogy of composite samples (wt. %). Pyrite, sphalerite, apatite, barite, rutile, and titanite are grouped as "others".**

| Mineral | Formula | Composition (wt.%) | | | | |
|---|---|---|---|---|---|---|
| | | C1 | C2 | C3 | C4 | C5 |
| Chalcocite | $Cu_2S$ | 1.2 | 0.2 | 1.6 | 1.5 | 0.7 |
| Bornite | $Cu_5FeS_4$ | 0.9 | 0.1 | 0.6 | 0.4 | 0.7 |
| Chalcopyrite | $CuFeS_2$ | 0.3 | 0.2 | 0.3 | 0.0 | 0.0 |
| Covellite | $CuS$ | 0.0 | 0.1 | 0.1 | 0.1 | 0.5 |
| Malachite | $Cu_2CO_3(OH)_2$ | 0.3 | 1.6 | 0.6 | 0.4 | 1.1 |
| Cuprite | $Cu_2O$ | 0.0 | 0.3 | 0.1 | 0.1 | 0.1 |
| Native Cu | $Cu$ | 0 | 0.1 | 0 | 0.1 | 0 |
| Quartz | $SiO_2$ | 41.6 | 11.5 | 35.2 | 36.6 | 34.2 |
| Dolomite | $CaMg(CO_3)_2$ | 19.5 | 75.0 | 20.9 | 23.5 | 23.3 |
| Biotite | $K(Mg,Fe)_3(OH,F)_2(Si_3AlO_{10})$ | 5.6 | 1.2 | 12.9 | 13.6 | 15.1 |
| Calcite | $CaCO_3$ | 5.3 | 0.4 | 3.4 | 3.0 | 6.3 |
| Orthoclase | $KAlSi_3O_8$ | 13.4 | 0.2 | 7.1 | 7.0 | 3.8 |
| Kaolinite | $Al_2Si_2O_5(OH)_4$ | 1.7 | 0.2 | 0.7 | 0.3 | 0.3 |
| Chlorite | $(Fe,Mg,Al)_6(Si,Al)_4O_{10}(OH)_8$ | 1.4 | 1.9 | 5.5 | 3.4 | 7.2 |
| Albite | $NaAlSi_3O_8$ | 4.5 | 0.3 | 3.7 | 2.6 | 4.0 |
| Muscovite | $KAl_2(AlSi_3O_{10})(OH,F)_2$ | 1.7 | 1.4 | 3.8 | 5.8 | 1.4 |
| Hematite | $Fe_2O_3$ | 0.4 | 2.3 | 0.6 | 0.1 | 0.2 |
| Goethite | $FeO(OH)$ | 0.0 | 0.3 | 0.1 | 0.0 | 0.0 |
| Iron oxide with Cu trace | $FeO(OH)\ Cu_X$ | 0.0 | 1.5 | 0.1 | 0.0 | 0.0 |
| Others | | 2.10 | 1.30 | 2.77 | 1.48 | 0.94 |
| **Mineral Total** | | **100.0** | **100.0** | **100.0** | **100.0** | **100.0** |

### 4.4.2. Cu distribution

Figure 7 illustrates the distribution of copper in the different composite samples. For C1, C3, and C4, chalcocite is the main copper-bearing mineral. It averages 52.3%, followed by bornite (18.5%) and malachite (13%). For C2, malachite constitutes more than 40% of the copper deportment, followed by chalcocite (35%), cuprite (9%), and bornite (2.5%). In C5, malachite represents around 40% of the total copper content, followed by chalcocite (24%), and bornite (17%). Chalcopyrite and covellite are not the main copper deportment in the characterized samples.

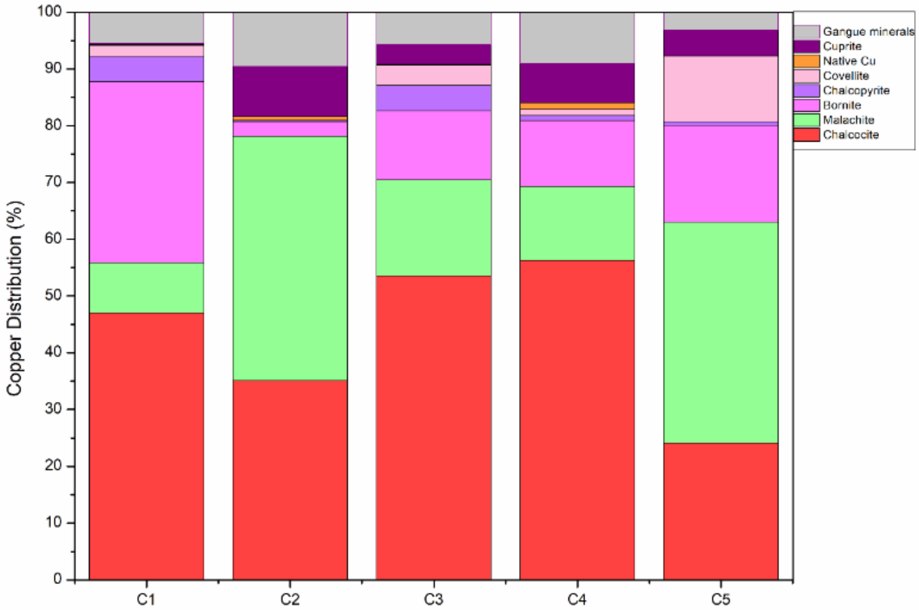


**Figure 7. Copper deportment mineral of composite samples (Quartz, calcite, dolomite, orthoclase, biotite, muscovite, and iron oxide are grouped as gangue minerals).**

Figure 7 illustrates an average of 6.5% of copper, distributed in gangue minerals, with a maximum of 10% for sample C2 and a minimum of 3% for sample C5, While the samples C4, C3, and C1 show respective percentages of 9%, 6%, and 5% of copper buried in mineral gangue as refractory copper.

In order to identify the gangue minerals carrying the refractory copper, a detailed mineralogical study was undertaken on the composite samples using SEM, EDS quantification, and EDS line scan analysis (Figure 8).

Atomic-scale EDS quantification results of the composite samples (Figure 8) showed a concentration of 1.68% of copper in dolomite, 6.34% in iron oxide, and 1.81% in muscovite with a homogeneous distribution according to the line scan performed on the same grains. The EDS quantification corresponds to spot centroid analysis conducted on individual grains of gangue minerals. The mineralogical characterization revealed that copper was buried as a solid matrix in gangue minerals when they were close to mineralization.

The mechanism responsible could be related to the strength of supergenesis. The supergene zone is divided into an enrichment zone and a leach cap. Commonly, the leach caps have the lowest copper value, while the enrichment zone has the highest copper concentration [26]. Under differentiation conditions, copper that was leached from copper bearing minerals could replace magnesium, iron or is absorbed by carbonate and silicate depending on the host rock. This fraction of copper is considered unrecoverable by the flotation process since the gangue minerals are not eligible to be adsorbed by the collector and constitutes crucial data for the mineralogical prediction of copper recovery. The refractory copper content for each composite is presented in Table 4.

**Table 4. Refractory copper content in composite samples.**

| Sample | *C1* | *C2* | *C3* | *C4* | *C5* |
|---|---|---|---|---|---|
| wt.% of refractory Cu | 0.06 | 0.1 | 0.05 | 0.09 | 0.03 |

### 4.4.3. Mineral liberation

The definition of liberation is based on area, whereas surface association is related to the perimeter of the particle of interest [27]. Depending on the association percentage of the grain perimeter with the background and the grinding mesh of samples, three classes are defined: liberated, middling, and locked, as illustrated in Figure 9.

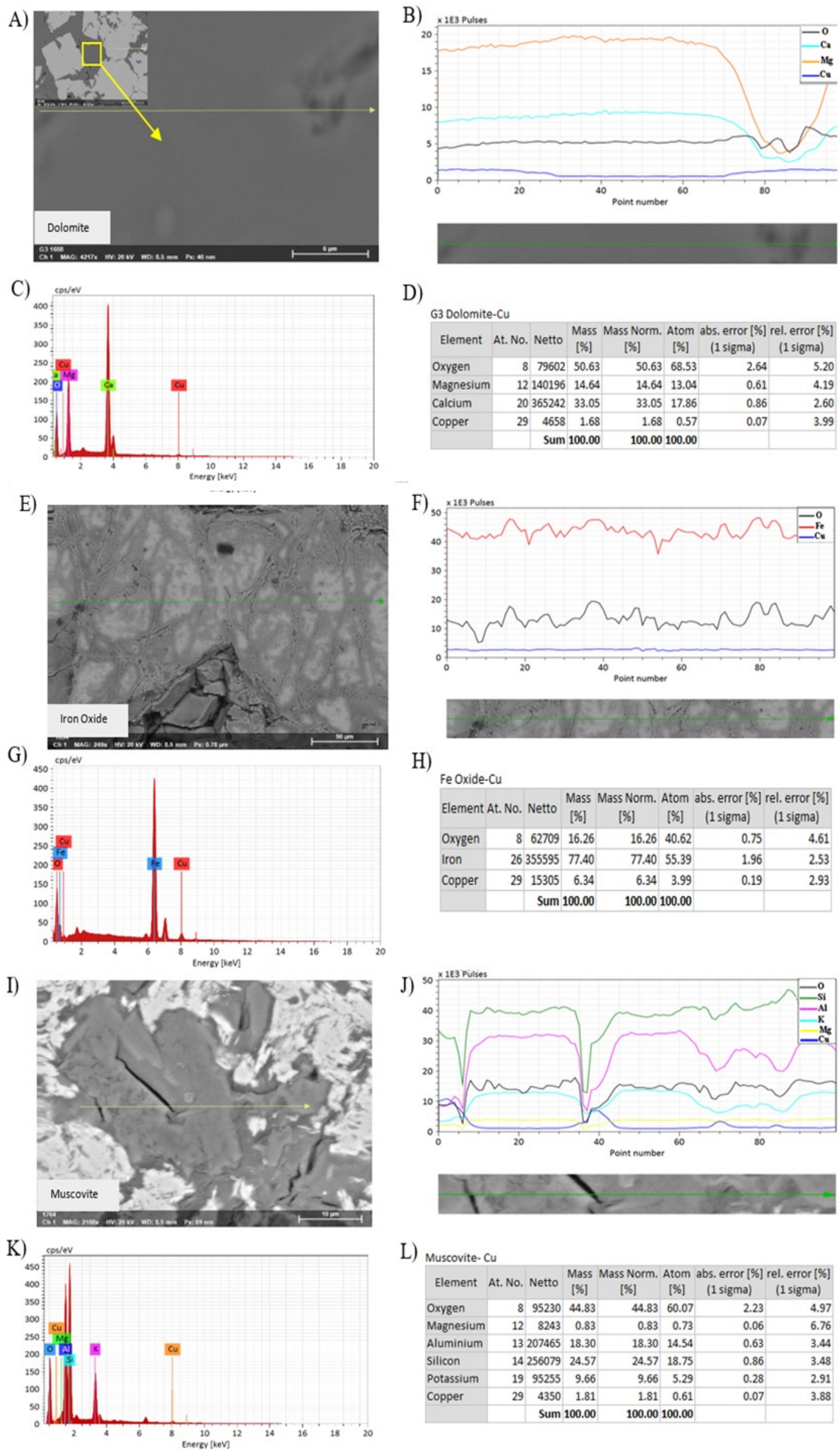


G3 Dolomite-Cu

| Element | At. No. | Netto | Mass [%] | Mass Norm. [%] | Atom [%] | abs. error [%] (1 sigma) | rel. error [%] (1 sigma) |
|---|---|---|---|---|---|---|---|
| Oxygen | 8 | 79602 | 50.63 | 50.63 | 68.53 | 2.64 | 5.20 |
| Magnesium | 12 | 140196 | 14.64 | 14.64 | 13.04 | 0.61 | 4.19 |
| Calcium | 20 | 365242 | 33.05 | 33.05 | 17.86 | 0.86 | 2.60 |
| Copper | 29 | 4658 | 1.68 | 1.68 | 0.57 | 0.07 | 3.99 |
| | | Sum | 100.00 | 100.00 | 100.00 | | |

Fe Oxide-Cu

| Element | At. No. | Netto | Mass [%] | Mass Norm. [%] | Atom [%] | abs. error [%] (1 sigma) | rel. error [%] (1 sigma) |
|---|---|---|---|---|---|---|---|
| Oxygen | 8 | 62709 | 16.26 | 16.26 | 40.62 | 0.75 | 4.61 |
| Iron | 26 | 355595 | 77.40 | 77.40 | 55.39 | 1.96 | 2.53 |
| Copper | 29 | 15305 | 6.34 | 6.34 | 3.99 | 0.19 | 2.93 |
| | | Sum | 100.00 | 100.00 | 100.00 | | |

Muscovite- Cu

| Element | At. No. | Netto | Mass [%] | Mass Norm. [%] | Atom [%] | abs. error [%] (1 sigma) | rel. error [%] (1 sigma) |
|---|---|---|---|---|---|---|---|
| Oxygen | 8 | 95230 | 44.83 | 44.83 | 60.07 | 2.23 | 4.97 |
| Magnesium | 12 | 8243 | 0.83 | 0.83 | 0.73 | 0.06 | 6.76 |
| Aluminium | 13 | 207465 | 18.30 | 18.30 | 14.54 | 0.63 | 3.44 |
| Silicon | 14 | 256079 | 24.57 | 24.57 | 18.75 | 0.86 | 3.48 |
| Potassium | 19 | 95255 | 9.66 | 9.66 | 5.29 | 0.28 | 2.91 |
| Copper | 29 | 4350 | 1.81 | 1.81 | 0.61 | 0.07 | 3.88 |
| | | Sum | 100.00 | 100.00 | 100.00 | | |

**Figure 8: Line scan of refectory Cu in mineral gangue. A) BSE photomicrograph of dolomite in association with malachite. B) Dolomite line scan with Cu trace; C and D) Dolomite EDS spectrometer. The quantification of refractory Cu in dolomite is around 1.68%. E) Iron oxide SEM image. (F) Line scan of iron oxide with a trace of refractory Cu. G and H) EDS spectrometer of iron oxide, the quantification of refectory Cu is about 6.34%, indicating that the iron was relatively replaced by copper. I) BSE photomicrograph of micas (muscovite) associated with chalcocite. J) Muscovite line scan with Cu trace. K and L) EDS spectrometer of muscovite. The quantification of refectory Cu in muscovite is about 1.81%.**

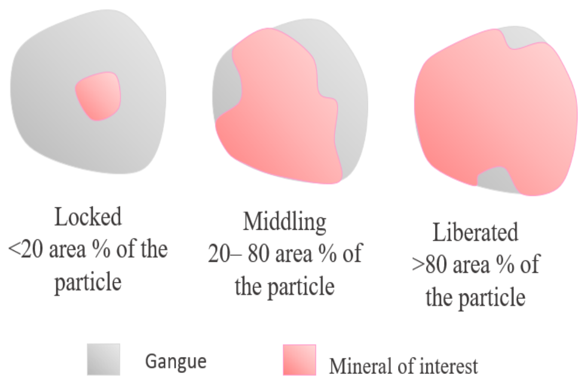


**Figure 9. Class particles are used to describe the liberation of a mineral of interest. The grinding mesh of the samples is 120 µm (modified after reference [28]).**

Considering the mineral abundance and Cu-distribution results, the liberation study was focused on the main copper-deportments: chalcocite, malachite, and bornite (Figure 10-A). Overall, total copper-deportment liberation was poor throughout the samples. The liberation rate average for composite samples is 22.5%, while the meddling grain rate averages 67.7%. The percentage of grain being locked shows a range of 7.2% for C4 and 13% for C2. According to Figure 11, the total copper content in locked classes shows a quite variable range. It is about 0.04 wt.% for sample C4, 0.06 wt.% for samples C1 and C3, and amounts to 0.08 wt.% for samples C2 and C5.

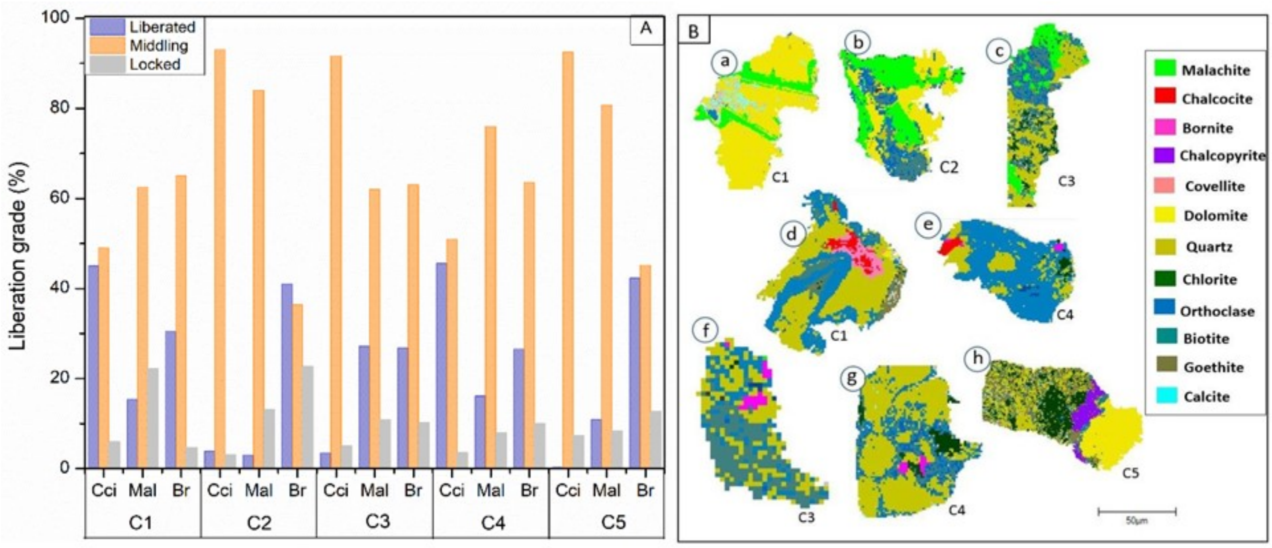


**Figure 10. A) Liberation data for major copper deportment in composite samples. B) Mineral maps for selected grains. Grains a and b: Malachite in association with dolomite. Grain c: Quartz and orthoclase grains with malachite association. Grain d: Chalcocite in association with covellite. The whole is included in the quartz. Grain e: Chalcocite in association with quartz and orthoclase. Grain f and g are composed of fine mosaics of quartz and biotite with bornite inclusions. Grain e: Chalcopyrite in association with dolomite and albite. Cci: Chalcocite; Mal: malachite; Br: bornite.**

In order to elucidate the impact of liberation on copper recovery performance, more detailed investigations were carried out on the locked class, allowing the distinction of two categories of locked copper (Figure 11). The first one is copper, locked in copper deportment. This fraction is considered available for collector adsorption and consequently recoverable by the flotation process. The second category is copper locked in gangue minerals. The copper rate recorded for this class varies between 37% (C2) and 67% (C5), implicating a copper content of 0.03wt.% and 0.05wt.%, respectively. This copper is considered unrecoverable since the surface area that is in contact with the collector is less than 20%.

Liberation is a fundamental metallurgical parameter for mineralogical prediction, notably the rate of copper being locked in gangue minerals. This data was used as the second input after the refractory copper for the prediction of copper recovery.

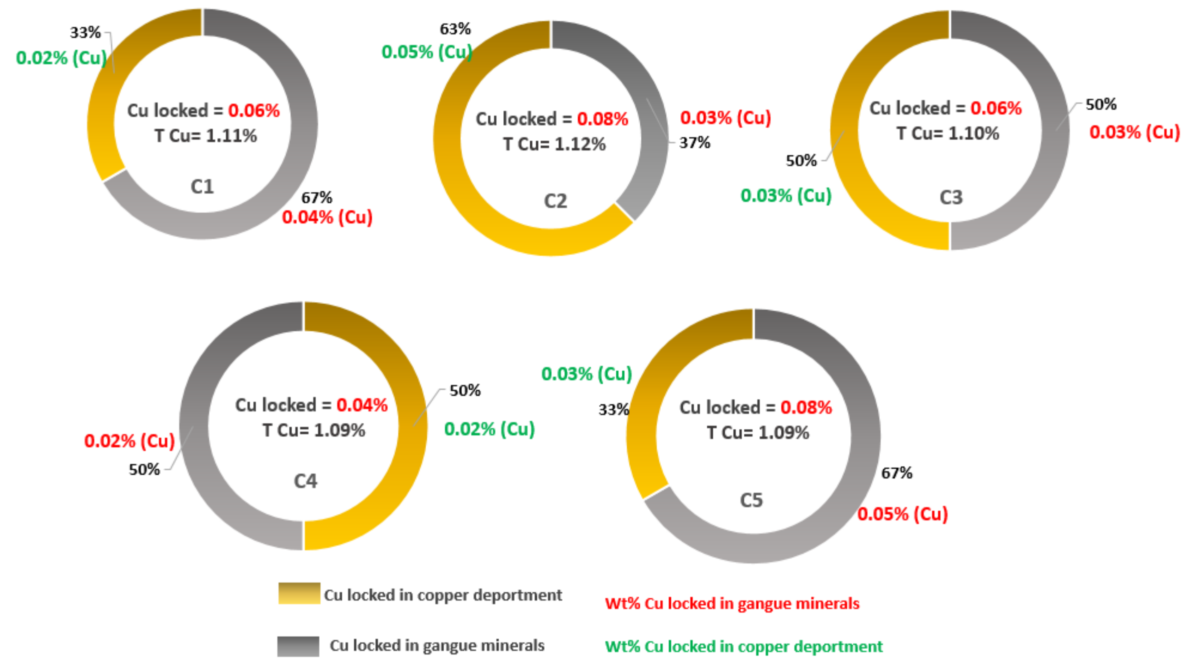


**Figure 11. Copper content distribution in grains locked in copper deportment and gangue minerals for composite samples.**

### 4.4.4. Flotation results

The grade-recovery performance of copper flotation for the composite samples is shown in Figure 12. The cumulative copper recovery for composite samples averages 92%, with an average grade of 23.5% Cu (Figure 11). The best copper recovery was observed for sample C5, with 95.6% and a grade of 26.49%. The lower grade-recovery was observed for sample C2. It is about 18.39% Cu and has a recovery rate of 89.67%. The copper recovery performances in the composite samples are very close due to their similar mineralogical composition such as the predominance of sulfides (chalcocite) and the presence of silico-carbonate gangue. Except for the sample C2, the gangue is mainly composed of dolomite (75%) and the copper deportments are mainly made up of carbonates (malachite) with a small amount of oxide (cuprite).

Compared to the low liberation rate, the significant percentage of mixed grain, and the proportion of locked particles, the flotation performance is very satisfactory in terms of recovery and copper grade.

### 4.5. Mineralogical prediction

The mineralogical prediction of copper recovery for composite samples was based on the liberation data, notably on copper content locked in the gangue and the refractory copper buried as a solid matrix in gangue minerals. Both of them were considered unrecoverable by the flotation process. The mineralogical copper recovery was calculated according to the equation illustrated in Figure 13.

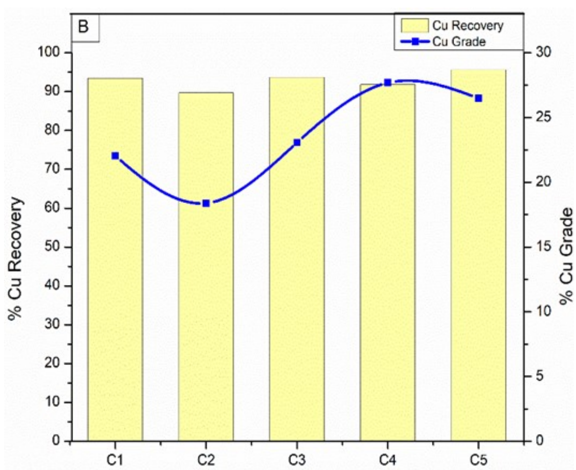


**Figure. 12. Global copper recovery versus copper grade in composite samples.**

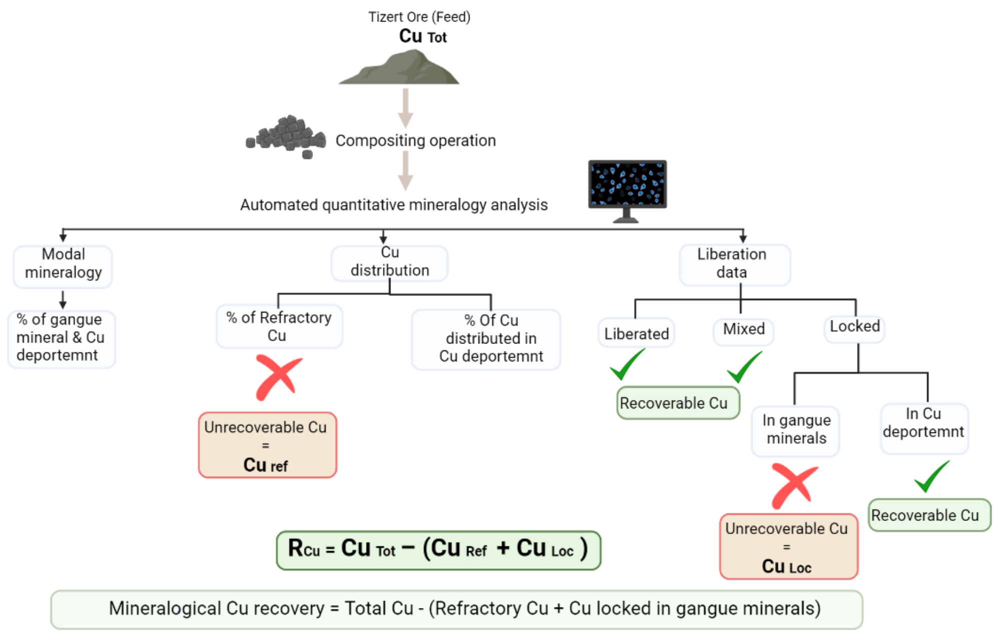


**Figure 13. Mineralogical prediction method based on AQM data.**

The correlation between the measured and predicted copper recoveries is illustrated in Table 5 and Figure 14. The predicted copper recovery averages 91.23%, with a maximum recovery of 93.58% for sample C5 and minimum recovery of 88.05% for sample C2. The measured and predicted copper recoveries are in good agreement with a maximum difference of 2.02%, an RMSE (Root Mean Square Error) of 1.64% and a $R^2$ value of 0.96. These results demonstrate that using the AQM data the copper recovery could be predicted accurately for the Tizert ore.

**Table 5. Correlation of measured and predicted copper recovery (with $p_i$ is the predicted value and $a_i$ is the measured value for n observations).**

| Samples | Cu recovery (predicted) % | Cu recovery (measured) % | Difference (%) | Squared residual |
|---|---|---|---|---|
| C1 | 91.89 | 93.44 | 1.55 | 2.40 |
| C2 | 88.05 | 89.67 | 1.62 | 2.61 |
| C3 | 92.73 | 93.64 | 0.91 | 0.83 |
| C4 | 89.91 | 91.81 | 1.90 | 3.62 |
| C5 | 93.58 | 95.60 | 2.02 | 4.09 |
| **RMSE** | $RMSE=\sqrt{\frac{\sum_{i=1}^{n}(p_i-a_i)^2}{n}}$ | | **1.64 %** | |

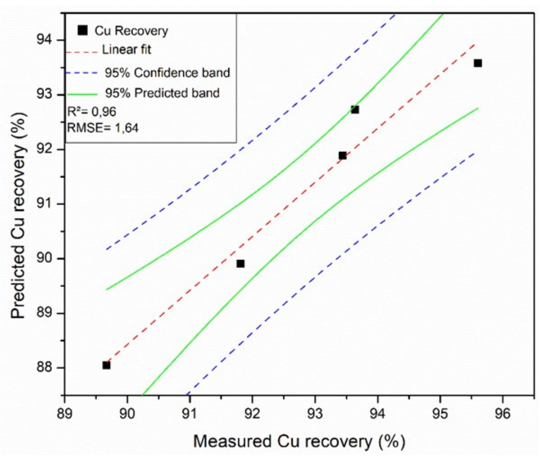


**Figure 14. Measured versus predicted copper recovery.**

## 5. Discussion

In this work, the prediction of metallurgical performance was investigated using the mineralogical approach. The applicability of the suggested method was tested on the Tizert deposit, in Western Anti-Atlas-Morocco. The goal was to take advantage of this approach in order to anticipate and predict the metallurgical performance of the Tizert ore in a more efficient and cost-effective way.

In this work, the metallurgical prediction of the Tizert ore was ensured by a combination of lithological field observation, microscopic characterization, and AQM analysis. The preliminary results of macroscopic observations performed on drill core demonstrate four morphological aspects of mineralized facies depending on the casing: massive in the conglomerates of the Basal Series, disseminated following the bedding of sandstones, stratified in the Tamjout dolomite, and fissural by sealing cracks in the Basal Series. The majority of the mineralization is carried out by chalcocite, bornite and malachite minerals. The mineralized facies aspect allows the affiliation of the mineralization to the sediment hosted-deposit type [9, 10]. Furthermore, the mineralogical characteristics of the Tizert deposit and their relationship with the casing are close to those reported in the sediment copper deposits of the Zambian Copperbelt [29].

The results of AQM performed on the composite samples were used for mineralogical prediction. The estimation of copper recovery was based on the liberation data, notably on unrecoverable copper locked in gangue minerals and the refractory copper buried as a solid matrix in gangue minerals. The results were compared with the flotation test work in order to ensure the validity of the method. The mineralogical copper recovery varied between 88.05% and 93.58%, achieving an average recovery above 91%, while the cumulative copper recovery by flotation test work averages 92% for composite samples. As a result, the flotation test work performance confirmed the findings of the mineralogical prediction. In addition, the correlation of measured and predicted copper recovery presented a coefficient of determination value of 0.96 and a RMSE of 1.67%. The past studies conducted on copper bearing minerals affirm the applicability of the mineralogical approach as a tool of investigation of flotation recovery [5]. The methodology consisted of the correlation of mineralogical characteristics with flotation performance in order to predict the recovery of the main copper minerals [5]. Other authors demonstrate the possibility of the application of this methodology as a tool for economic performance assessment [30]. The proposed model was based on the integration of liberation data, class characteristics, and the size and grade of sulfide minerals in order to create a predictive model for flotation recovery. Furthermore, the mineralogical approach linked to the metallurgical performance investigations could be used as a decision making tool by the companies [31].

This research work provided many interesting findings but there are some challenges that could be faced. Firstly, the representativeness of selected samples is important since quantitative mineralogy is performed on a limited number of samples. Secondly, the characterization of bulk mineralogy is slow and expensive, especially when mineralogy is variable and complex. Lastly, if additional zones are discovered, the whole model is required to be calibrated to the new mineralogical variability, which implies additional mineralogical characterizations. Finally, in order to adapt the applicability of the recommended model to an industrial scale, it is required to examine the operational differences between the laboratory bench scale and industrial operations. Considering all of these challenges will make the model more robust, resilient, and adaptive for all stages of the geo-metallurgical study including exploration, processing, and beneficiation.

## 6. Conclusions

In this work, the mineralogical approach was used as a tool for the geo-metallurgical prediction of the Tizert copper deposit in order to make early metallurgical predictions, provide quick and cost-effective data for geometallurgical study, and ensure visibility throughout the life of the mine. For this aim, a mineralogical approach based on the mineralogical bulk data was used.

The lithological observations and detailed mineralogical characterization performed on the Tizert ore samples produced precious mineralogical information that served as the input for AQM. Within this deposit, chalcocite, malachite, and bornite are the main copper deportments being hosted in a silico-carbonate gangue. In order to establish the validity of the proposed method, the flotation test work was performed on the Tizert composite samples at the optimal operating conditions. This work demonstrates that the predicted copper recovery and flotation test results are in good agreement with a maximum difference of 2.02%, an RMSE of 1.64%, and an $R^2$ value of 0.96. As a result, it is possible to predict the metallurgical recovery throughout the Tizert deposit using the mineralogical data. Furthermore, an early prediction of the flotation performance is very useful in the geo-metallurgical model conception and persepectives. On a larger scale, the applicability of this model can be extended by incorporating the mineralogical approach into all steady-state processes in order to cover all the probable mineralogical variabilities during the operations and to provide an industrial process control.

## Acknowledgments

The authors gratefully acknowledge the REMINEX research center for the financial support and analysis, especially Mr. Mohamed Belghiti and Mr. Abdelmaoula Mouahid for their assistance and support.

## References

[1]. Lamberg, P. (2011). Particles-the Bridge between Geology and Metallurgy. In Conference in Minerals Engineering. Luleå.

[2]. Lishchuk V., Lamberg P., and Lund C. (2015). Classification of geometallurgical programs basedon approach and purpose. The 12th Biennial SGA Meeting, Nancy, France. 4pp.

[3]. Lamberg, P.(2013). Building a Geo-metallurgical Model in Iron Ores using a Mineralogical Approach with Liberation Data. The second AUSIMM international geometallurgy conference/ Brisbane, QLD, pp. 317–324.

[4]. Tijsseling, L,T., Dehaine, Q., Rollinson, G,K., and Glass, H,J. (2020). Mineralogical Prediction of Flotation Performance for a Sediment-Hosted Copper–Cobalt Sulphide Ore. Minerals, 10, 474.

[5]. Rincon, J., Gaydardzhiev, S., and Stamenov, L. (2019). Investigation on the flotation recovery of copper sulphosalts through an integrated mineralogical approach. Miner. Eng., 130, 36–47.

[6]. Little, L., Mclennan, Q., Prinsloo, A., Muchima, K., Kaputula, B., and Siame, C. (2018). Relationship between ore mineralogy and copper recovery across di_erent processing circuits at Kansanshi mine. J. S. Afr. Inst. Min. Metall, 118, 1155–1162.

[7]. Pouit, G. (1966). Paleogeographie et repartition des mineralisations stratiformes de cuivre dans l'Anti-Atlas occidental (Maroc), Chron. Rech. Min, 34, 279-289.

[8]. Fauvelet, E. (1971). Réflexion sur une liaison possible entre minéralisation cuprifère et roches plutoniques basiques hercyniennes dans l'Anti-Atlas (Maroc). Colloque scientifique international, Raguin, Paris, Masson 1971.

[9]. Oummouch, O., Essaifi, A., Zayane, R., Maddi, O., Zouhair, M., and Maacha, L. (2017). Geology and Metallogenesis of the Sediment-Hosted Cu-Ag Deposit of Tizert (Igherm Inlier, Anti-Atlas Copperbelt, Morocco). Hindawi, Vol. 2017, 19pp.

[10]. El Basbas, A., Aissa, M., Ouguir, H., Mahdoudi, M.L., Maddi, A., and Zouhair, M. (2020). Ouansimicopper mineralization (Western Anti-Atlas, Morocco): Paragenetic sequence and circulationof gangue hosted paleofluids., J. Afr. Earth Sci. 162, 103692, 64pp.

[11]. Thomas, R.J., Fekkak, A., Ennih, N., Errami, E., Loughlin, S.C., Gresse, P.G., Chevallier, L. P., and Liégeois, J.P. (2004). A new lithostratigraphic framework for the Anti-Atlas Orogen, Morocco. J. Afr. Earth Sci. 39 (3–5), 217–226.

[12]. Oudra, M., Beraaouz, H., Ikenne, M., Gasquet, D., and Soulaimani, A. (2005). La tectonique panafricaine du secteur d'Igherm : implication des dômes extensifs tardi à post-orogéniques (Anti-Atlas Occidental, Maroc). Estud. Geol. 61 (3–6), 177–189.

[13]. Hafid, A. (1992). Granites et dolérites protérozoïques de la boutonnière d'Igherm (Anti- Atlas Occidental) (Pétrologie, géochimie et signification géodynamique). PhD Dissertation. Pierre and Marie Curie Université.

[14]. Soulaimani, A. (1998). Interactions socle/couverture dans l'Anti-Atlas Occidental (Maroc): rifting fini-Protérozoïque et orogenèse hercynienne. PhD Dissertation. Caddi Ayyad University, Marrakech-Morocco.

[15]. Choubert, G. and Faure Muret, A. (1973). Nouvelles données sur les massifs précambriens des Ida Ou-Zeddoute et des Ida Ou-Zekri ; NW d'Igherm ; Anti-Atlas (Maroc). C. R. Acad. Sci. Paris 276 (4), 477–480.

[16]. Hefferan, K.P., Karson, J.A., and Saquaque, A. (1992). Proterozoic collisional basins in a Pan-African suture zone, Anti-Atlas Mountains, Morocco. Precambrian Res. 54, 295–319.

[17]. Thomas, R.J., Fekkak, A., Ennih, N., Errami, E., Loughlin, S.C., Gresse, P.G., Chevallier, L.P., and Liégeois, J.P. (2004). A new lithostratigraphic framework for the Anti-Atlas Orogen, Morocco. J. Afr. Earth Sci, 39, 217–226.

[18]. Gasquet, D., Levresse, G., Cheilletz, A., Azizi-Samir, M.R., and Mouttaqi, A. (2005). Contribution to a geodynamic reconstruction of the Anti-Atlas (Morocco) during Pan-African times with the emphasis on inversion tectonics and metallogenic activity at the Precambrian-Cambrian transition. Precambrian Res. 140, 157–182.

[19]. Maloof, A.C., Schrag, D.P., Crowley, J.L., and Bowring, S.A. (2005). An expanded record of Early Cambrian carbon cycling from the Anti-Atlas Margin, Morocco. Can. J. Earth Sci. 2005, 42, 2195–2216.

[20]. Demange, M. (1980.) Stratigraphie, volcanisme et paléogéographie du Précambrien III et de la série de base dans la partie sud de la boutonnière d'Ouaouafenrha (Anti-Atlas occidental). Notes et Mémoires du Service Géologique du Maroc, Vol. 41, pp. 7–23.

[21]. Poot, J.,Verhaert, M., Dekoninck, A.,Oummouch, A.,El Basbas, A., Maacha, L., and Yans, J. (2020). Characterization of Weathering Processes of the Giant Copper Deposit of Tizert (Igherm Inlier, Anti-Atlas, Morocco). Minerals, 10, 620.

[22]. Yasrebi, A.B., Hezarkhani, A., Afzal, P., Karami, R., Eskandarnejad Tehrani, M., and Borumandnia, A. (2020). Application of an Ordinary Kriging-Artificial Neural Network for Elemental Distribution in Kahang Porphyry Deposit, Central Iran. Arabian Journal of Geosciences 13, 748 (1-14).

[23].Benssaou, M. and Hamoumi, N. (2001). L'Anti Atlas occidental du Maroc: étude sédimentologique et reconstitution paléogéographique au Cambrien inférieur. Journal of African Earth Sciences, Vol. 32, pp. 351–372.

[24]. Algouti, A.J. Beauchamp, J., Chbani, B., and Taj-Eddine, K. (2000). Paléogéographie d'une plateforme infracambrienne en dislocation : série de base adoudounienne de la région Waoufengha–Igherm, Anti-Atlas occidental, Maroc. Comptes Rendus de l'Académie des Sciences - Series IIA - Earth and Planetary Science, Vol. 330, No. 2, pp. 155–160.

[25]. Anhaeusser, C. R. and Button.A. (1973). A petrographic and mineragraphic study of the copper-bearing formations in the Witvlei area, south West Africa. Economic Geology Research Unit, Univ. of the Witwatersrand, Johannesburg, South Africa. 21pp.

[26]. Sillitoe, R H. and McKee, E H. (1996). Age of supergene oxidation and enrichment in the Chilean porphyry copper province. Economic Geology. Vol. 91, 164-179 pp.

[27]. Becker, M., Harris, P.J., Wiese, J.G., and Bradshaw, D.J. (2009). Mineralogical characterisation of naturally floatable gangue in Merensky Reef ore flotation. Int. J. Miner. Process. 93, 246–255.

[28]. Pillay, K. (2015). Mineralogical effects on the dense medium separation of low grade nickel sulphide ore. PhD Dissertation. University of Cape Town South Africa. 200pp.

[29]. Selley, D., Broughton, D., Scott, R,. Hitzman, M., Bull, S., Large, R., McGoldrick, P., Croaker, M, and Pollington N. (2005). A new look at the geology of the Zambian Copperbelt, Economic Geology, pp.965–1000.

[30]. Zhang, J. and Subasinghe, N. (2016). Development of a flotation model incorporating liberation characteristics. Miner. Eng. 98, 1–8.

[31]. Ntlhabane, S., Becker, M., Charikinya, E., Voigt, M., Schouwstra, R., and Bradshaw, D. (2018). Towards the development of an integrated modelling framework underpinned by mineralogy. Miner. Eng. 116, 123–131.

# رویکرد کانی شناسی - ابزاری برای پیش بینی ژئو متالورژیکی کانسار مس Tizert (ایغرم داخلی، آنتی اطلس، مراکش)

کائوتار داچری[1*]، خالد ناجی[2]، کلثوم نوار[2]، انتصار بنزکر[2]، خالد أوزیه[2]، مصطفی بدری[2]، عبدالمالک بوستی[2]، حکیم فقیر[2]، خالد إل أمری[1] و محمد هیبتی[1]

۱- دانشگاه کادی ایاد، FST مراکش، مراکش
۲- مرکز تحقیقات Reminex، مراکش

ارسال ۲۰۲۱/۰۱/۱۵، پذیرش ۲۰۲۲/۰۳/۱۵

* نویسنده مسئول مکاتبات: dachri.kaoutar@gmail.com

**چکیده:**

هدف این کار تعریف یک ابزار کارآمد و نوآورانه به منظور پیش‌بینی‌های متالورژیکی اولیه از کانسار Tizert در غرب مراکش است. برای انجام این کار، رویکرد کانی شناسی به‌عنوان ابزاری برای پیش‌بینی ژئومتالورژیکی با استفاده ترکیبی از مشاهدات صحرایی، سنگ‌شناسی مغره‌های حفاری، مشاهدات میکروسکوپی بر روی ۵۴ مقطع نازک، و کانی‌شناسی (AQM) انجام‌شد که تمامی آنها بر روی پنج نمونه مرکب مورد بررسی قرار گرفت. پیش‌بینی متالورژیکی سنگ معدن Tizert بر اساس داده‌های آزادسازی است، به ویژه بر روی محتوای مس موجود در باند و مس غیرقابل بازیافت که به‌عنوان یک ماتریس جامد در کانی‌های بانگ (مس نسوز) مدفون شده است. به منظور اطمینان از اعتبار روش پیشنهادی، نتایج پیش‌بینی کانی شناسی با نتایج بدست آمده از آزمایش فلوتاسیون مقایسه شد. در نتیجه، نتایج بازیافت مس پیش‌بینی‌شده از داده‌های کانی‌شناسی عملاً مشابه نتایج به‌دست‌آمده از آزمایش‌های فلوتاسیون است که حداکثر اختلاف ۰/۰۲٪، مقدار R2 = 96/0، و ریشه میانگین مربعات خطای ۱/۶۴٪ را نشان می‌دهد. این نتایج نشان داد که با استفاده از داده های AQM، بازیابی مس را می‌توان به طور دقیق برای سنگ معدن Tizert پیش‌بینی کرد. علاوه بر این، پیش‌بینی اولیه عملکرد فلوتاسیون در مفهوم مدل ژئو متالورژیکی بسیار مفید است. علاوه بر این، چنین رویکردی در طول عمر معدن داده‌های سریع و مقرون به صرفه را برای پردازش عملکرد فراهم می‌کند. در مقیاس صنعتی، کاربرد این روش را می‌توان با ادغام رویکرد کانی‌شناسی در تمام فرآیندهای حالت پایدار به منظور پوشش تنوع کانی‌شناسی احتمالی در طول عملیات و تضمین کنترل فرآیند صنعتی گسترش داد.

**کلمات کلیدی:** کانی شناسی کمی خودکار، Tizert، مس، ژئومتالورژی، مراکش.